

Interannual variability and predictability of summertime significant wave heights in the western North Pacific

Wataru Sasaki

Storm, Flood and Landslide Research Department,
National Research Institute for Earth Science and Disaster Prevention,
3-1 Tennodai, Tsukuba, Ibaraki 305-0006, Japan
email: wsasaki@bosai.go.jp

Toshiyuki Hibiya

Department of Earth and Planetary Science, Graduate School of Science,
The University of Tokyo, Tokyo, Japan

1 INTRODUCTION

Many authors have presented studies on the interannual variability, long-term trend, and extremes of significant wave heights (SWH) using buoy observations, altimeter measurements, and wave reanalyses. In particular, much effort has been devoted to studies of the wintertime wave climate in the North Atlantic. Using the longest-running wave record in the world, Carter and Draper (1988) and Bacon and Carter (1991) presented the 0.034 m/yr upward trend of SWH at the Seven Stones Light Vessels off the SW coast of England since 1962. A strong relationship between the wintertime wave climate in the North Atlantic and the North Atlantic Oscillation (NAO) was identified (WASA group, 1998; Wang and Swail, 2001; Woolf et al., 2002). Furthermore, Woolf et al. (2002) proposed a statistical model using the NAO index to predict SWH in the North Atlantic. Caires and Sterl (2004) estimated global 100-year return values of SWH and wind speed by applying the peaks-over-threshold method to the ERA-40 wave reanalysis, which is produced by the European Centre for Medium-Range Weather Forecasts (ECMWF) as a part of the 40-year reanalysis (ERA-40) project.

Changes in the wave climate in the North Pacific have also been investigated, with an emphasis on the relationship between wintertime wave climate and winter storm activity. Allan and Komar (2000) presented the increase of buoy SWH on the coast of California in the eastern North Pacific during major El Niño events as well as an apparent upward trend

over the last two decades. Based on the wave reanalysis obtained from the third generation wave model, WaveWATCH III (Tolman, 1999), Graham and Diaz (2001) and Graham et al. (2002) clarified the long-term upward trend of SWH in the northern storm track as evidence of an increase in winter storm activity. Yamaguchi and Hatada (2002) found an upward trend of both wind speed and SWH in the northern area of the Western North Pacific (WNP) during 1948-1998 using a wave reanalysis based on the shallow water wave model. Kako and Kubota (2006) examined the relationship between interannual variability of wintertime SWH in the North Pacific and El Niño events by applying an EOF analysis to optimally interpolated monthly mean TOPEX/Poseidon SWH data.

Although the changes of wintertime wave climate have thus been extensively analyzed, changes of summertime wave climate have not been fully investigated. In the boreal summer, high waves caused by tropical cyclones (TCs) have a severe impact on the coastal areas of eastern Asia. It is important to clarify the relation between the wave climate in the WNP and the TC activity.

This paper has a dual purpose. The first is to clarify the interannual variability of summertime SWH in the WNP. The second is to construct a linear regression model to predict SWH and to assess the performance of the regression model.

The rest of this paper comprises six sections. Section 2 describes datasets and applied procedures. Section 3 is devoted to an analysis of the interannual

variability of SWH in the WNP. Section 4 presents a relationship between the interannual variability of SWH and TC activity. In Section 5 we propose and validate a regression model that enables us to predict SWH in the WNP. Section 6 presents a summary and discussion.

2 DATASETS

2.1 ERA-40 WAVE REANALYSIS

To investigate the interannual variability of SWH, we need to use SWH data covering the long-term without any spatial or temporal gaps. In addition, it is desirable that the wave data be free of inhomogeneity caused by changes of instruments and/or observation technique. We use two different wave reanalyses: the ERA-40 wave reanalysis (Uppala et al., 2005) and the optimally interpolated TOPEX/Poseidon SWH data.

The ERA-40 wave reanalysis, produced by the ECMWF, covers the entire globe on a $2.5^\circ \times 2.5^\circ$ latitude-longitude grid for Sep 1957 - Aug 2002 at 6-hour intervals. The main feature of the ERA-40 wave reanalysis is that ERS-1 and ERS-2 wave measurements are assimilated from Dec 1991 and Jun 1996 onward, respectively. The accuracy of the ERA-40 wave reanalysis has been validated against buoy, ERS-1, and TOPEX altimeter measurements (Caires and Sterl, 2003) as well as other wave reanalyses (Caires et al., 2004).

We prepared the monthly 90th percentile of SWH for Jan 1960 - Aug 2002 (H_{90e}). Although the ERA-40 wave reanalysis has high accuracy, we exclude H_{90e} for Dec 1991 - May 1993 from the datasets since the ERA-40 wave reanalysis has inhomogeneities during this period due to the assimilation of faulty ERS-1 Fast Delivery Product (Bauer and Staabs, 1998).

2.2 OPTIMALLY INTERPOLATED TOPEX/POSEIDON WAVE DATA

2.2.1 PROCEDURE

In this section we introduce our optimally interpolated TOPEX/Poseidon monthly 90th percentile SWH data (OITP wave data). To produce the OITP wave data, we employ the TOPEX/Poseidon along-track, quality-checked, deep-water altimeter measurements of SWH for repeat cycles 11-453, covering the period Jan 1993 - Dec 2004. The TOPEX/Poseidon SWH data are obtained from the NASA Physical Oceanography Distributed Active Archive Center at the Jet Propulsion Laboratory/California Institute of Technology. The TOPEX is a dual-frequency altimeter, while the Poseidon is an experimental altimeter used only occasionally during

the mission. In the present study, we use the data obtained by the Ku-band altimeter of the TOPEX.

The TOPEX datasets are decoded using the recommended quality controls described in the TOPEX documentation. SWH from the TOPEX measurements are overestimated for Feb 1997 - Feb 1999 compared to SWH from the ERS-2 measurements. This overestimate was identified as an electronics drift of the TOPEX altimeter. By fitting an exponential curve to the SWH data, Queffelec (1999) proposed a method to correct the TOPEX SWH drift such that

$$SWH_{\text{corr}} = SWH + h,$$

where

$$h = \exp\left(\sum_{i=0}^{i=3} (a_i \times 98^i)\right) - \exp\left(\sum_{i=0}^{i=3} (a_i \times c^i)\right),$$

$$a_0 = -1.00935 \times 10^{-2},$$

$$a_1 = -4.75094 \times 10^{-2},$$

$$a_2 = 3.10926 \times 10^{-4},$$

$$a_3 = -5.15826 \times 10^{-7},$$

$$98 \leq c \leq 235.$$

In these formulas, SWH denotes the original TOPEX SWH, SWH_{corr} denotes the corrected TOPEX SWH, and c denotes the TOPEX cycle number. We apply this correction relationship to the TOPEX SWH for cycles 98-235. The monthly 90th percentile of SWH on each $1^\circ \times 1^\circ$ grid is calculated after this correction.

Figures 1a and 1b show maps of the 90th percentile of TOPEX SWH for Jan 2004 and for Jul 2004, respectively. A number of gaps and artificial patterns attributable to satellite tracks are found, especially in the northern and southern mid-latitudes and western North Pacific. To fill the gaps and remove the artificial patterns, we apply an optimal interpolation (OI) method to the gridded monthly 90th percentile of SWH (H_{90t}). The OI method is extensively used as an interpolation technique in the oceanic and atmospheric sciences. Kako and Kubota (2006) recently presented a global gridded monthly mean SWH dataset for 1993-2002 by applying an optimal interpolation (OI) method to the TOPEX/Poseidon SWH. They showed that the monthly mean of TOPEX SWH interpolated by the OI method agrees with that of buoy SWH better than simple monthly mean TOPEX SWH in terms of month-to-month variability.

We set the spatial correlation scale (e-folding scale) to 1500 km and 1000 km for longitudinal and latitudinal directions, respectively. These values are the same as those used by Kako and Kubota (2006). Figures 1c and 1d show maps of the 90th percentile of the

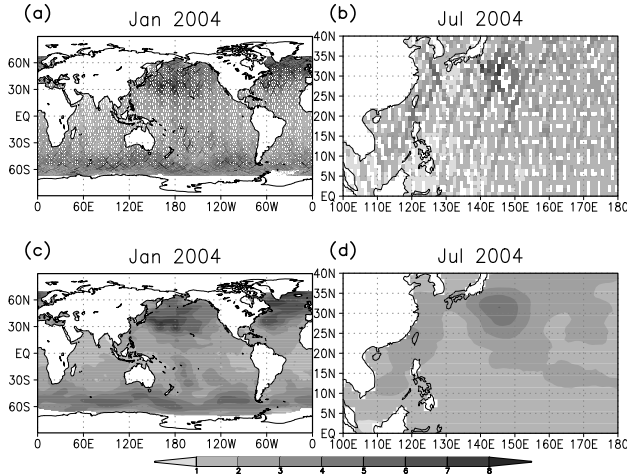


Figure 1: (a) Monthly 90th percentile of the TOPEX significant wave heights for January 2004 without spatial interpolation. Gaps in the ocean show the lack of the TOPEX altimeter measurements. (b) As in (a), but for July 2004 in the western North Pacific. (c) and (d) As in (a) and (b), respectively, but with the optimal interpolation method.

optimally interpolated TOPEX SWH for Jan 2004 and for Jul 2004, respectively, where artificial patterns are removed and gaps are interpolated by the OI method.

2.2.2 VALIDATION OF OITP WAVE DATA

To check the validity of the OITP wave data, we employ buoy wave observations for Jan 1994 - Dec 2001, obtained from the National Oceanic and Atmospheric Administration's National Data Buoy Center. The buoy SWH are calculated by averaging the highest one-third of the sea surface elevation for the 20-minute records.

We select a total of 14 buoys for validation: four buoys around the Hawaii Islands (buoys 51001, 51002, 51003, and 51004), one buoy around the coast of Alaska (46001), three buoys in the northeastern Pacific (46002, 46005, and 46006), three buoys in the Gulf of Mexico (42001, 42002, and 42003), and three buoys in the northwestern Atlantic (41001, 41002, and 44004) (Fig. 2). The buoy selection criteria are based on the water depth, since the TOPEX/Poseidon altimeter measures SWH in the open ocean. We prepare the monthly 90th percentile of buoy SWH for each buoy (H_{90b}).

To validate the OITP wave data against the buoy observations, we present the correlation coefficient (ρ) between H_{90t} and H_{90b} , the bias (H_{90t} minus H_{90b}), and the root-mean-square (rms) errors for each

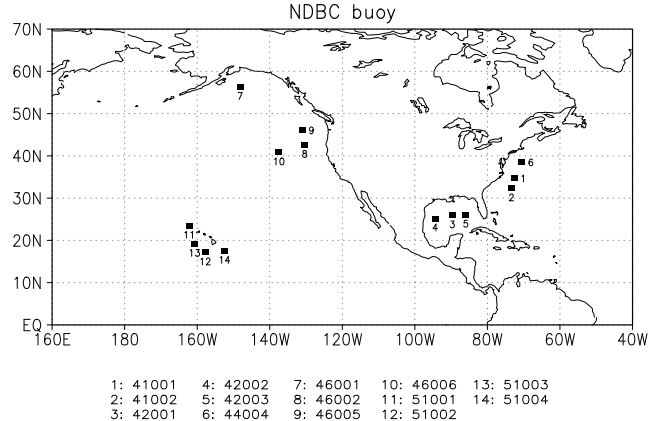


Figure 2: Locations of the NDBC buoys (square mark). Each number corresponds to the buoy number shown below the map.

buoy. For reference, the ERA-40 wave reanalysis is also statistically compared with the buoy observations. The period of the comparison is 96 months (12 month \times 8 years) from Jan 1994 to Dec 2001.

Table 1 provides the statistical comparisons of H_{90b} with each of H_{90t} and H_{90e} . The correlations between H_{90t} and H_{90b} and between H_{90e} and H_{90b} both exceeded 0.8 for all of the buoys except buoy 51001, indicating that the OITP wave data and/or the ERA-40 wave reanalysis both agree well with the buoy observations in terms of the month-to-month variability.

The OITP wave data and the ERA-40 wave reanalysis are negatively biased by about 0.3 m and 0.45 m, respectively, showing that the OITP wave data agrees with the buoy observations better than the ERA-40 wave reanalysis in terms of the bias.

The rms errors between the OITP wave data and the buoy observations are smaller than those between the ERA-40 wave reanalysis and the buoy observations, indicating that the OITP wave data agrees with the buoy observations better than the ERA-40 wave reanalysis in terms of the magnitude of month-to-month variability.

The above results indicate that the quality of the OITP wave data compares favorably with that of the ERA-40 wave reanalysis. To examine the interannual variability of high sea states in boreal summer, we prepare the 3-month (June-August) mean of the monthly 90th percentile of SWH (H_{90}) for each year. Hereafter, we use the term H_{90t} and H_{90e} to denote H_{90} for the OITP wave data and H_{90} for the ERA-40 wave reanalysis, respectively.

2.3 ADDITIONAL DATA

To identify the atmospheric anomalies associated with the interannual variability of H_{90} in the WNP,

Buoy		ρ	Bias	Rms	Buoy		ρ	Bias	Rms
41001	OITP	0.87	-0.35	0.62	46001	OITP	0.97	-0.48	0.63
	ERA	0.91	-0.49	0.68		ERA	0.95	-0.78	0.92
41002	OITP	0.83	-0.15	0.49	46002	OITP	0.96	-0.38	0.62
	ERA	0.88	-0.33	0.52		ERA	0.98	-0.48	0.63
44004	OITP	0.93	-0.15	0.30	46005	OITP	0.97	-0.28	0.50
	ERA	0.95	-0.29	0.39		ERA	0.97	-0.51	0.65
42001	OITP	0.88	-0.20	0.34	46006	OITP	0.96	-0.37	0.58
	ERA	0.92	-0.40	0.47		ERA	0.98	-0.56	0.68
42002	OITP	0.91	-0.34	0.44	51001	OITP	0.68	-0.47	0.83
	ERA	0.95	-0.44	0.48		ERA	0.66	-0.51	0.86
42003	OITP	0.88	-0.46	0.72	51002	OITP	0.93	-0.46	0.50
	ERA	0.91	-0.36	0.62		ERA	0.93	-0.58	0.62
					51003	OITP	0.96	-0.28	0.37
						ERA	0.94	-0.39	0.46
					51004	OITP	0.94	-0.30	0.37
						ERA	0.94	-0.34	0.42
The North Atlantic Ocean					The North Pacific Ocean				
OITP					OITP				
0.88					0.92				
-0.27					-0.38				
0.49					0.55				
ERA					ERA				
0.92					0.92				
-0.38					-0.52				
0.53					0.66				
Mean for all buoys									
OITP					OITP				
0.90					-0.33				
0.52					0.60				
ERA					ERA				
0.92					-0.46				
-0.46					0.60				

Table 1: Statistical comparison of the wave data from the buoy observations with each of the OITP wave data and the ERA-40 wave reanalysis. Bold numbers correspond to the closest agreement with each buoy observation. Unit for the bias and the rms error is m.

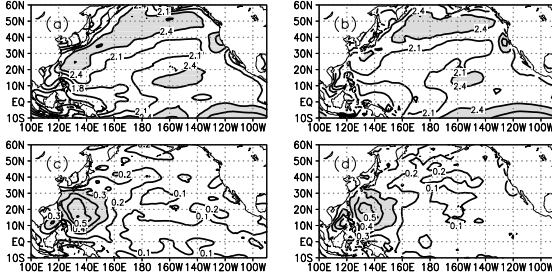


Figure 3: (a) A map showing the climatological June-August mean of the monthly 90th percentile of significant wave heights for 1993-2002 based on the optimally interpolated TOPEX/Poseidon significant wave height. Unit is m. Contour interval is 0.3. The areas where the value exceeds 2.4 are shaded. (b) As in (a), but based on the ERA-40 wave reanalysis for 1993-2002. (c) A map showing the standard deviation of H_{90t} for 1993-2002. Contour interval is 0.1. Unit is m. The areas where the values exceed 0.3 are shaded. (d) As in (c), but for H_{90e} for 1993-2002.

we employ 10-m surface wind (SW) fields and sea level pressure (SLP) fields obtained from the ERA-40 reanalysis for 1960-2002 as well as those obtained from the National Centers for the Environmental Prediction/National Centers for Atmosphere Research (NCEP/NCAR) reanalysis for 1993-2004. To identify sea surface temperature (SST) anomalies associated with the interannual variability of H_{90} in the WNP, we use SST fields for 1960-2004 obtained from the Extended Reconstructed SST dataset described by Smith and Reynolds (2004). We prepare 3-month (June-August) averaged maps of these variables for each year.

To examine the relationship between the interannual variability of H_{90} and the TC activity in the WNP, we use TC best-track data for 1960-2002 compiled by the Regional Specialized Meteorological Center (RSMC) Tokyo Typhoon Center. The RSMC best-track data includes the name of TC as well as positions (latitude and longitude) and central surface pressure of TC at every 6-hour (sometimes 3-hour) intervals.

To quantify TC activity, we define the following two variables as indices. The first is the TC frequency, which is calculated by summing the number of TC passing over the region 0° - 30° N, 120° E- 160° E during June-August. The second is a total duration of intense TC (ITC; with central pressure less than 980 hPa), which is calculated by summing the duration of each ITC within the region 0° - 30° N, 120° E- 160° E during June-August. Both variables are used by Sasaki et al. (2005b), who presented evidence of

an increase in extreme wave heights in the WNP since the late 1990's.

3 INTERANNUAL VARIABILITY OF SUMMERTIME SIGNIFICANT WAVE HEIGHTS

Figures 3a and 3b show maps of the climatological mean of H_{90t} and H_{90e} , respectively. The climatological mean of H_{90e} is smaller than that of H_{90t} by about 0.3 m in the WNP. Figures 3c and 3d show the standard deviation of H_{90t} and that of H_{90e} , respectively. It can be seen that the standard deviation of H_{90t} is greater than that of H_{90e} by about 0.1 m in the WNP. All of these results are consistent with the statistical comparison shown in Table 1. Although there is a difference in the standard deviation between H_{90t} and H_{90e} , both datasets suggest that the standard deviation of H_{90} is notably large in the WNP. We set the region 0° - 40° N, 100° E- 180° E as our main analysis domain.

First, we examine the interannual variability of H_{90} for 1993-2004 based on the OITP wave data. To identify the most prevailing interannual variability of H_{90t} within the analysis domain, we apply an Empirical Orthogonal Function (EOF) analysis to H_{90t} based on the covariance matrix. The first EOF mode accounts for 66.9% of the total variance within the analysis domain, which is much larger than the second mode (10.3%) and third mode (5.1%). The third mode does not show apparent signal in the WNP, so we focus only on the first and second EOF modes hereafter.

Figure 4a shows a map of linear regression coefficients between H_{90t} and the first principal component (PC1) of H_{90t} . The spatial pattern of the linear regression coefficients is characterized by a monopole structure with the maximum amplitude located to the south of Japan. This location of the maximum amplitude seems to correspond to the region where TCs develop their intensity (Fig. ??). Figure 4b shows a normalized time series of the PC1 of H_{90t} where the prominent interannual variability can be recognized. It is interesting to note that large positive anomalies occur, mainly during the El Niño/Southern Oscillation (ENSO) developing years (Chou et al., 2003), i.e., 1997 and 2002. This is consistent with the fact that SWH off Hiratsuka and at Irozaki show large positive anomalies in 1997 and 2002 (Fig. ??). A large positive anomaly of the PC1 of H_{90t} is also found in 2004 (Fig. 4b). This could be caused by a large number of TC passing over the WNP. A total of 10 TCs (the largest number since 1951) made landfall on Japanese islands in 2004.

Typical SST anomalies associated with the interan-

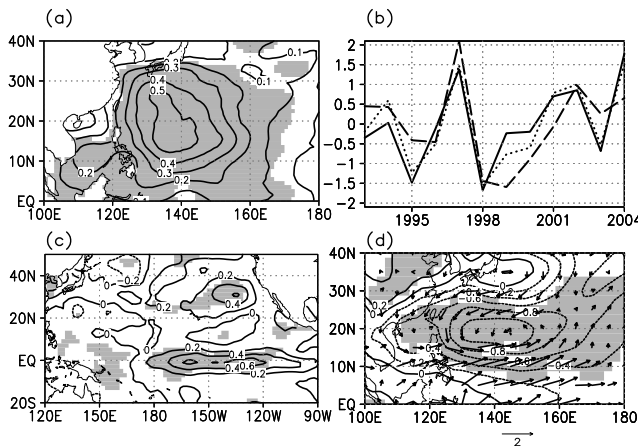


Figure 4: (a) A map showing linear regression coefficients between H_{90t} (m) and the first principal component (PC1) for H_{90t} . Shaded areas indicate the correlation exceeds 99% significance. (b) The normalized time series of the PC1 for H_{90t} (solid line), Niño-3.4 index (dashed line), and U_{10N} (dotted line). U_{10N} is defined as zonal wind anomalies averaged over the region 5°N - 15°N , 130°E - 160°E . The Niño-3.4 index and U_{10N} are based on the ERSST and the NCEP/NCAR reanalysis, respectively. (c) A map showing the linear regression coefficients between SST and the PC1 of H_{90t} (degC). Shaded areas indicate that the correlation exceeds 99% significance. (d) A map showing the linear regression coefficients between the PC1 of H_{90t} and each of SLP (contour) and surface wind (arrow). Unit of SLP is hPa. Shaded areas indicate the correlation exceeds 99% significance.

nual variability of H_{90t} are identified in a map of linear regression coefficients between SST and the PC1 of H_{90t} (Fig. 4c), where we find that the PC1 of H_{90t} is positively correlated with SST in the equatorial central Pacific. The temporal evolution of SST averaged over the Niño-3.4 region (Niño-3.4 index) is similar to that of the PC1 of H_{90t} (Fig. 4b). In fact, the correlation coefficient between the PC1 of H_{90t} and the Niño-3.4 index is 0.68, indicating that interannual variability of H_{90t} in the WNP links with the ENSO events. Although the year 2004 is not recognized as an ENSO year, the spatial pattern of warm SST anomalies in the central equatorial Pacific resembles that of an ENSO year.

Figure 4d shows a map of linear regression coefficients between the PC1 of H_{90t} and each of SW and SLP of the NCEP/NCAR reanalysis, where we find that typical atmospheric anomalies associated with the interannual variability of H_{90t} are characterized

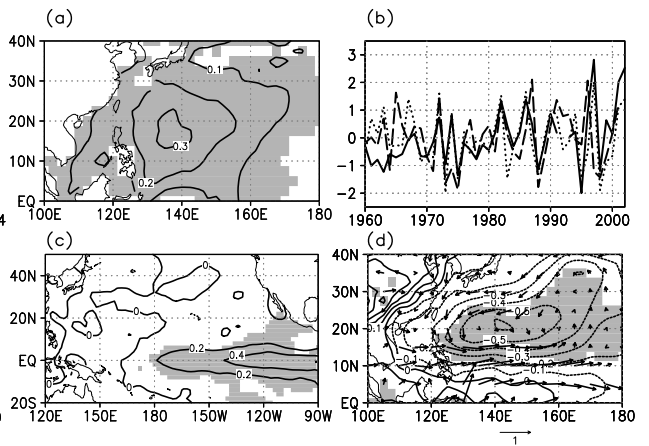


Figure 5: As in Fig. 4, but for H_{90e} .

by the counter-clockwise SW anomalies and negative SLP anomalies in the WNP. A striking feature of the SW anomalies is anomalous westerly winds within the region 5°N - 15°N , 130°E - 160°E (Fig. 4d). This motivates us to introduce an index defined by averaging zonal winds over the region 5°N - 15°N , 130°E - 160°E (U_{10N}). The time series of U_{10N} coincides with that of the PC1 of H_{90t} (Fig. 4b). The correlation coefficient between the PC1 of H_{90t} and U_{10N} for 1993-2004 is 0.95.

The above analysis period (12-yr) is not long enough to clarify the relationship between the interannual variability of H_{90} in the WNP and the ENSO events. To remedy this, we use the ERA-40 wave reanalysis for 1960-2002. The analysis domain is the same as that an EOF analysis is applied to H_{90t} . We apply an EOF analysis to H_{90e} for 1960-2002 based on the covariance matrix. The first EOF of H_{90e} accounts for 51% of the total variance within the analysis domain, which is much larger than the explained variance of the second mode (13%) and third mode (5.5%), so that we focus only on the first EOF mode.

The spatial pattern of the first EOF mode of H_{90e} is consistent with that of H_{90t} (Figs. 4a and 5a), but the regression coefficients of H_{90e} are smaller than those of H_{90t} by about 0.2 m. This discrepancy may be caused by the difference of the analysis period as well as the difference between the standard deviation of H_{90t} and that of H_{90e} in the WNP (Figs. 3c and 3d). Temporal evolution of the PC1 of H_{90e} is characterized by large positive anomalies during the ENSO developing years, i.e., 1972, 1982, 1986, 1991, 1997, and 2002 (Fig. 5b). This is consistent with the result that the PC1 of H_{90t} tends to increase during the ENSO developing years.

Typical SST, SW, and SLP anomalies associated

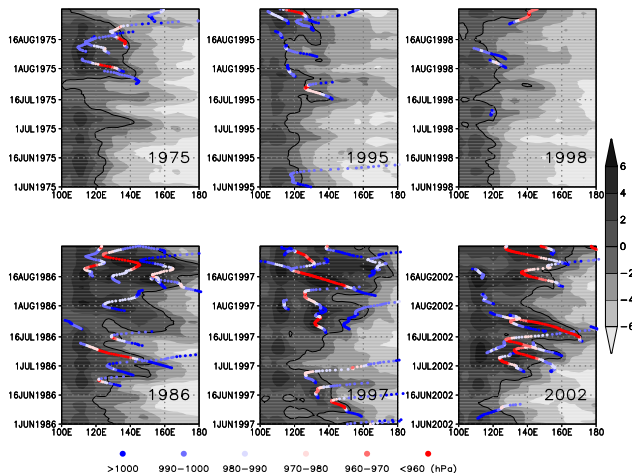


Figure 6: Time-longitude section of TC's position (colored circle) as well as 5-day moving average of zonal winds (ms^{-1}) averaged over the latitudinal band 5°N - 15°N (shade) during three low PC1 of H_{90e} years (upper panels) and three high PC1 of H_{90e} years (lower panels). Bold contour shows zero. Color of the circle corresponds to the central pressure of TC shown on the bottom.

with the PC1 of H_{90e} (Figs. 5c and 5d) agree very well with those associated with the PC1 of H_{90t} (Figs. 4c and 4d). The decadal correlation coefficients between the PC1 of H_{90e} and the Niño-3.4 index are shown in Table 2a, which shows that they are poorly correlated during 1960-1969 ($\rho = -0.16$), but much improved after 1970 ($\rho \geq 0.5$). Table 2b indicates that the PC1 of H_{90e} and U_{10N} are closely correlated with each other after 1970 ($\rho > 0.7$), consistent with the fact that the PC1 of H_{90t} is closely correlated with U_{10N} . Thus, the robust relationship between the PC1 of H_{90} and U_{10N} can be confirmed in terms of the OITP wave data as well as the ERA-40 wave reanalysis. This result allows us to use U_{10N} as a predictor for the PC1 of H_{90} in the WNP. Poor correlations between the PC1 of H_{90e} and each of the Niño-3.4 index and U_{10N} during 1960-1969 are discussed in Section 6.

It is interesting to note that the spatial pattern of the first EOF mode of H_{90e} is not explained adequately by an increase of the westerly winds at latitude around 10°N . On the other hand, the position of the maximum amplitude of the first EOF mode of H_{90e} located to the south of Japan corresponds to the region where TCs frequently pass through and develop their intensity. In the next section, we investigate the relationship among the first EOF mode of H_{90e} , anomalous westerly winds at 10°N , and TC

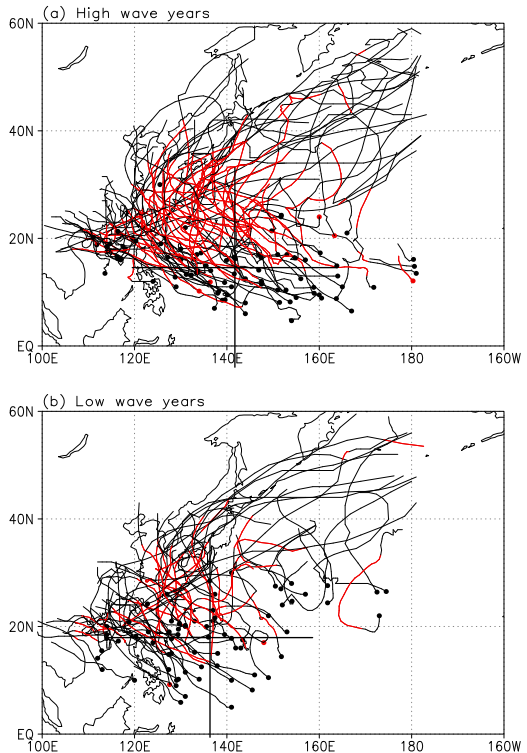


Figure 7: Map showing the locations of TC occurrence and the TC tracks during the highest 7 years of the PC1 of H_{90e} (a) and during the lowest 7 years of the PC1 of H_{90e} (b). Each closed circle shows the position of TC occurrence. TC tracks along which the TC's central pressure is below 980 hPa are red-colored. The horizontal and vertical lines show the mean latitude and longitude of TC occurrence, respectively, with the intersection located at 15.1°N , 141.5°E (a) and 17.9°N , 136.3°E (b).

activity.

4 TROPICAL CYCLONE ACTIVITY

In this section, we focus on the relationship between the first EOF mode of H_{90} and TC activity. The anomalous westerly winds causing an increase of H_{90} in the WNP may be associated with an eastward extension of the monsoon trough off the east of the Philippines, which brings about an eastward shift of TC occurrence. Figure 6 shows the time-longitude section of TC's position and zonal winds averaged over the latitudinal band 5°N - 15°N . During the three years of the low PC1 of H_{90e} (1975, 1995, and 1998), TCs tend to occur west of 140°E in accordance with weak westerly winds. In addition, most of the TCs do not develop the intensity (upper panels in Fig. 6). In contrast, during the three years of the high PC1 of

	Period				
	1960–1969	1970–1979	1980–1989	1990–2002	1960–2002
(a)	−0.16	0.60	0.67	0.56	0.49
(b)	0.00	0.88	0.77	0.83	0.66
(c)	0.22	0.68	0.81	0.81	0.63
(d)	0.21	0.44	−0.14	0.38	0.02

Table 2: Decadal correlation coefficients between the PC1 of H_{90e} in the western North Pacific and (a) the Niño-3.4 index, (b) U_{10N} , (c) total duration of ITC, and (d) TC frequency.

H_{90e} (1986, 1997, and 2002), TCs tend to occur further east area in accordance with the strong westerly winds, and develop the intensity due to the long duration (lower panels in Fig. 6). These results suggest that interannual variability of U_{10N} which is closely related to the interannual variability of H_{90} in the WNP affects the position of TC occurrence and TC development.

We compare the position of TC occurrence and TC development during the high wave years with those during the low wave years. The high wave years and the low wave years are designated based on the PC1 of H_{90e} ; we focus on seven high (low) wave years showing the highest (lowest) seven PC1 of H_{90e} . Figure 7 shows a comparison between TC occurrence and TC development during the high wave years and those during the low wave years. The mean position of the TC occurrence shifts about 3° southward and 5° eastward during the high wave years relative to those during the low wave years. It is notable that more TCs occur east of 140°E and south of 10°N during the high wave years than during the low wave years. This result is supported from the correlations between the PC1 of H_{90e} and TC occurrence on a $12.5^\circ \times 20^\circ$ latitude-longitude grid in the WNP (Fig. 8). We can see that TC occurrence in the region 0° – 12.5°N , 140°E – 160°E is correlated with the PC1 of H_{90e} .

Considering that the PC1 of H_{90e} is closely correlated with the ENSO events, these results are consistent with the fact that the position of TC occurrence shifts south-eastward during strong ENSO events (Wang and Chan, 2002). This implies that TCs occur further away from the continents, so they may have longer duration until they encounter the continent or cool mid-latitude water. As Wang and Chan (2002) report, TCs tend to increase their intensity in proportion to their duration.

We also find another marked difference in TC activity between the high wave years and the low wave years. Although most of TCs are found to pass by the south of Japan during both the high wave years and the low wave years (Fig. 7), we can see a marked

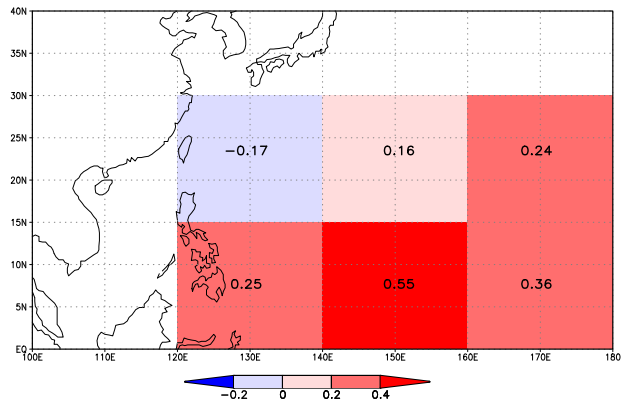


Figure 8: Correlation coefficients between PC1 of H_{90e} and TC occurrence on a $12.5^\circ \times 20^\circ$ latitude-longitude grid during 1970–2002.

difference between the frequency of intense TC (ITC, TC with the central pressure below 980 hPa) during the high wave years and that during the low wave years. During the high wave years, a relatively large number of ITCs is found to pass by the south of Japan (see red lines in Fig. 7a). The area where the ITCs frequently pass agrees with the area where amplitude of the first EOF mode of H_{90} is large. This result suggests that the first EOF mode of H_{90} is dominated by the ITC activity in the WNP.

The relationship between the interannual variability of H_{90e} and ITC activity can be examined using two TC indices, viz., the total duration of ITC and the frequency of TC occurrence. Table 2c provides the decadal correlation coefficients between the PC1 of H_{90e} and the total duration of ITC, where we can see that their correlation is much closer after 1970 ($\rho > 0.6$). In contrast, Table 2d shows that the frequency of TC occurrence and the PC1 of H_{90e} are not correlated with each other. This is consistent with the findings of Sasaki et al. (2005a), who showed that the observed interannual variability of SWH off the southern coast of Japan is more closely related to the ITC activity rather than the frequency of TC

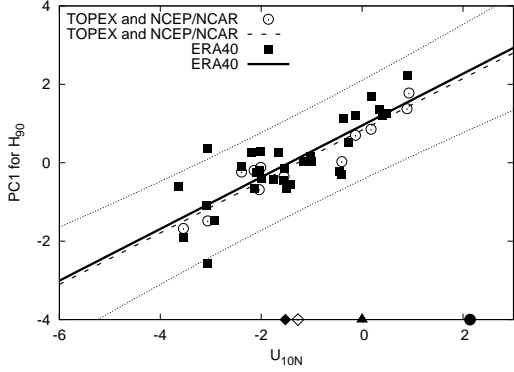


Figure 9: Relationship between the PC1 of H_{90} in the western North Pacific and U_{10N} obtained from the ERA-40 reanalysis (square) as well as that obtained from the optimally interpolated TOPEX/Poseidon wave data and the NCEP/NCAR reanalysis wind data (circle). Our regression model is represented by a straight line obtained from the least square fit. The solid line is for the ERA-40 reanalysis, whereas the dashed line is for the TOPEX/Poseidon wave data and the NCEP/NCAR reanalysis wind data. Dotted lines show the 95% predictive interval. The open and filled diamond shows climatological summer mean of U_{10N} obtained from the ERA-40 reanalysis during 1970-2002 and that obtained from the NCEP/NCAR reanalysis during 1993-2004, respectively. The triangle and filled circle shows the 10-yr mean of U_{10N} obtained from the control run and the $2 \times CO_2$ run, respectively.

occurrence in the WNP. Sasaki et al. (2005b) also showed that the recent increase of summertime SWH in the WNP is mainly due to the increase of ITC activity rather than the frequency of TC occurrence.

5 VALIDATION OF THE REGRESSION MODEL

Figure 9 shows the linear relationship between the PC1 of H_{90} in the WNP and U_{10N} obtained from the ERA-40 reanalysis as well as from the OITP wave data and the NCEP/NCAR reanalysis winds. Note that we use H_{90e} during 1970-2002, since the relationship between the PC1 of H_{90e} and U_{10N} is poor during 1960-1969. Using the least squares method, the regression model based on the ERA-40 wave reanalysis during 1970-2002 is given by

$$PC1' = 0.66 \times U_{10N} + 0.95, \quad (1)$$

where $PC1'$ denotes the PC1 of H_{90} predicted by U_{10N} . On the other hand, a regression model based

on the OITP wave data and the NCEP/NCAR reanalysis winds during 1993-2004 is given by

$$PC1' = 0.66 \times U_{10N} + 0.83. \quad (2)$$

It should be noted that the slopes of the two regression models obtained from the different datasets are nearly identical, suggesting that the relationship between the PC1 of H_{90} in the WNP and U_{10N} is robust. Although we can find a small bias (0.12 m) between the two regression models (1) and (2), the predicted values of H_{90} are not severely affected by it.

We now evaluate the performance of the regression model obtained from the ERA-40 wave reanalysis as well as from the OITP wave data. To assess the performance of the regression model, we calculate the rms errors between H_{90} and H_{90} reconstructed by the U_{10N} index (H_{90}^R) which is given by

$$H_{90}^R = EOF1 \times PC1'_1, \quad (3)$$

where EOF1 denotes the regression coefficients between H_{90} and the PC1 of H_{90} .

The rms error between H_{90} and H_{90}^R (Δ) can be estimated by

$$\Delta = \sqrt{\sum_{\text{year}} (H_{90} - H_{90}^R)^2 / N}, \quad (4)$$

where N denotes the number of years. Predictability of H_{90} using U_{10N} index is estimated by the following formulation, indicating percentage of the H_{90} variance explained by use of U_{10N} index.

$$(1 - \Delta / \sqrt{\sum_{\text{year}} H_{90}^2 / N}) \times 100(\%) \quad (5)$$

Using the U_{10N} index, H_{90} within the latitudinal band $10^\circ N$ - $25^\circ N$ is successfully reconstructed by up to 40% for the ERA-40 wave reanalysis (Fig. 10a), and by up to 70% for the OITP wave data (Fig. 10c). Our regression model is thus shown to be successful to reproduce H_{90} considerably, though errors exceeding 0.3 m still remains, particularly in the East China Sea.

6 SUMMARY AND DISCUSSION

We have investigated the interannual variability of the summer (June-August) mean of the monthly 90th percentile of significant wave heights (H_{90}) in the western North Pacific (WNP) using the ERA-40 wave reanalysis and the optimally interpolated TOPEX/Poseidon (OITP) significant wave height

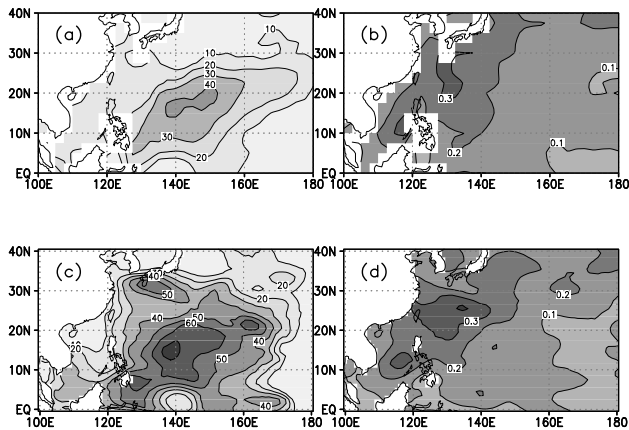


Figure 10: (a) Percentage of the H_{90e} variance explained by the variability estimated using U_{10N} index. (b) The rms errors between H_{90e} and H_{90e} reconstructed by U_{10N} index. Unit is m. (c) As in (a), but for H_{90t} . (d) As in (b), but for H_{90t} .

data. We have clarified that an increase in the first principal component (PC1) of H_{90} is closely correlated with an increase in ITC activity which links with the positive zonal wind anomalies averaged over the region 5°N - 15°N , 130°E - 160°E (U_{10N}) during ENSO developing years.

The positive U_{10N} anomaly may be associated with an eastward extension of the monsoon trough off the east coast of the Philippines, which causes an eastward shift of TC occurrence. In fact, the mean position of TC occurrence during the typical seven high wave years shifts southeastward compared to that during the typical seven low wave years, so that TCs further develop while traveling longer distances until they encounter the continent or cool mid-latitude water. This explains the close correlation between the PC1 of H_{90} and the total duration of ITCs.

Based on these results, we have proposed a linear regression model which enables us to predict H_{90} in the WNP in terms of U_{10N} . It has been shown that the linear regression model obtained from the ERA-40 reanalysis and that obtained from the OITP wave data and the NCEP/NCAR reanalysis are nearly identical. The performance of the U_{10N} index has been assessed in terms of the percentage of the H_{90} variance explained by use of U_{10N} index. The predictor has been found to be successful to reproduce H_{90} by up to 40% for the ERA-40 wave reanalysis and by up to 70% for the OITP wave data, though rms errors exceeding 0.3 m still remain in the East China Sea.

The relatively large rms errors between H_{90e} and

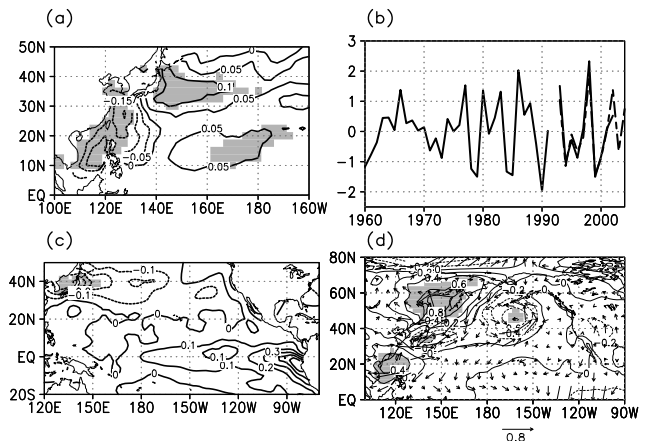


Figure 11: As in Fig. 5, but for the second mode. Solid and dashed lines in (b) show normalized time series of the principal component of the second EOF mode of H_{90e} from the ERA-40 and the OITP data, respectively.

H_{90e} reconstructed by using the U_{10N} index are observed in the East China Sea (see Fig 10b). Even for the rms errors between H_{90e} and H_{90e} reconstructed by using the PC1 of H_{90e} , the large errors still remain there (Fig. not shown). This result suggests that the rms errors in the East China Sea are due to neglect of the higher EOF modes of H_{90e} variability rather than due to the skill of the U_{10N} index. We, therefore, examine here the second EOF mode of H_{90e} which explains 13% of the total variance.

The spatial structure of the second EOF mode of H_{90e} is characterized by negative anomalies in the East China Sea, positive anomalies in a region east of Japan, and a region within 10°N - 20°N , 160°E - 180° (Figure 11a). In particular, the anomaly of H_{90e} in the East China Sea is relatively larger than that in the other regions.

It is interesting to note that the PC2 of H_{90e} increases during the years after the El Niño, namely, 1966, 1977, 1983, 1988, 1993, and 1998 (Fig. 11b). Most of these years correspond to cool summers in northern Japan characterized by an increase of Yamase, cold northeasterly winds over northern Japan. Kanno (2004) showed that a pressure difference between Wakkanai and Sendai as an index of Yamase increased during 1983, 1988, 1993, and 1998. Figure 11c showing a regression map between SST and the PC2 of H_{90e} also supports the increase in the PC2 of H_{90e} are correlated with negative SST anomalies around Japan.

Figure 11d shows a linear regression map between the PC2 of H_{90e} and each of SW and SLP anoma-

lies. Typical atmospheric anomalies associated with an increase in the PC2 of H_{90e} is characterized by positive SLP anomalies in the East China Sea and the Sea of Okhotsk, and by negative SLP anomalies over Japan and a region located to the south of Aleutian Islands. Anomalous northeasterly cold winds associated with the positive SLP anomalies over the Sea of Okhotsk may cause negative SST anomalies around Japan (Figs. 11c and 11d), and relatively strong SW over the East/South China Sea and the region near Japan results in the large SWH in these particular regions. It is also interesting to note that the spatial pattern of the SLP anomalies is similar to the Pacific-Japan pattern presented by Nitta (1987). Further investigations about the second EOF mode of H_{90} remains to be studied in the future.

To predict H_{90} accurately, regression coefficients between H_{90} and the PC1 of H_{90} are crucial. Although the regression model for the ERA-40 wave reanalysis and that for the OITP wave data and the NCEP/NCAR reanalysis are nearly identical (Fig. 9), some difference exists between the regression coefficients of H_{90e} and those of H_{90t} (Figs. 4a and 5a). In this study, we employed the original ERA-40 wave reanalysis, which is most widely used. Caires and Sterl (2003) pointed out that the original ERA-40 wave reanalysis overestimates low wave heights and underestimates high wave heights. The underestimate of high wave heights may result in the existing difference between the regression coefficients of H_{90e} and those of H_{90t} . Caires and Sterl (2005) applied a statistical correction to the original ERA-40 wave reanalysis to show that the agreement with buoy observations can be improved. There is also some ambiguity in the OITP wave data; a $1^\circ \times 1^\circ$ grid may have few satellite passes over each grid point per month, which inevitably introduces some bias, especially for high sea states in the monthly wave climatology. Thus, possible statistical corrections of H_{90e} as well as more accurate estimates of H_{90t} remain as a topic for future study to improve the prediction accuracy for H_{90} .

Considering that it is difficult to produce accurate simulations of the observed TC occurrence, TC development and TC tracks using the current global climate models, our simple regression model is believed to greatly contribute to the prediction of future significant wave heights in the WNP. Houghton et al. (2001) in the IPCC reports documented that several global climate models predict that as global temperatures increase under the effect of greenhouse gases, the Pacific SST field will exhibit an ENSO-like pattern (Knutson and Manabe, 1995; Mitchell et al., 1995; Meehl and Washington, 1996; Timmermann et al., 1999; Boer et al., 2000). It follows that summertime SWH in the WNP will increase under global

warming conditions. We should bear in mind, however, that this prediction is based on the assumption that the statistical relationship between the PC1 of H_{90} and U_{10N} for the last three decades will hold, even under future climate conditions.

As shown in Table 2, the PC1 of H_{90e} during 1960-1969 shows poor correlations with each of the U_{10N} index, the Niño-3.4 index, and total duration of ITC. There may be two possible reasons of the poor correlations. The first reason is the quality of the datasets. Although satellite wave observations are assimilated into the ERA-40 wave model from 1992 to 2002, the wave model is driven only by sea surface winds of the ERA-40 reanalysis during other periods. Even though the data for other variables observed by satellite are assimilated into the atmospheric model from the 1980's, quality of the ERA-40 wave reanalysis may be worse before 1980 than after 1980. In addition, the poor correlations during 1960-1969 may also come from the quality of the best-track data, since satellite monitoring of the weather events over the WNP began in 1964. The second reason of the poor correlations between the PC1 of H_{90e} and other indices during 1960-1969 may be attributable to climate change. Applying an EOF analysis to H_{90e} for 1960-1969 indicates that the third principal component of H_{90e} correlates well with the U_{10N} index ($\rho = 0.87$), which suggests that the relationship between U_{10N} and the most prevalent mode of interannual variability of H_{90} changed during the late 1960's. Further investigations into the causes of the poor correlations during 1960-1969 remain to be studied in the future.

This paper has been restricted to the study on the interannual variability of the summertime SWH in the open ocean. As a next step of this study, it is worthwhile to study wave climate in other seasons and in regions near the coast, in detail. For example, waves are strongly affected by northwesterly winds and extra-tropical storms during winter in the Sea of Japan. Similarly, high high waves at the southern coast of Japan in winter are caused mainly by the passage of the extra-tropical storms. Sasaki et al. (2005) presented that the wintertime (December-February) SWHs off Hiratsuka after 1987 have increased compared to those before 1986. In contrast, such change of the wintertime SWHs has not been detected at Irozaki which is located about 100 km southwest to Hiratsuka. This may be due to the difference of the location of the observation points. Hiratsuka is located to the head of Sagami bay, while Irouzaki is located to the mouth of Sagami bay. This suggests that the shape of the bay is also an important factor for the regional wave climate. In addition, the accurate wind fields with fine resolution should be

required to investigate the regional wave climate.

7 ACKNOWLEDGEMENTS

This work was partially supported by the Global Environment Research Fund (S-5(3)) of the Ministry of the Environment, Japan.

REFERENCES

- Allan, J. C., and P. D. Komar, 2000: Are ocean wave heights increasing in the eastern North Pacific?, *Eos, Transactions, American Geophysical Union*, **47**, 561–567.
- Bacon, S., and D. J. T. Carter, 1991: Wave climate changes in the North Atlantic and North Sea, *Int. J. Clim.*, **11**, 545–558.
- Bauer, E., and C. Staabs, 1998: Statistical properties of global significant wave heights and their use for validation, *J. Geophys. Res.*, **103**, 1153–1166.
- Boer, G. J., G. Flato, and D. Ramsden, 2000: A transient climate change simulation with greenhouse gas and aerosol forcing: projected climate for the 21st century, *Clim. Dyn.*, **16**, 427–450.
- Caires, S., A. Sterl, 2003: Validation of ocean wind and wave data using triple collocation, *J. Geophys. Res.*, **108**, 3098, doi:19.1029/2002JC001491.
- Caires, S. and A. Sterl, 2004: 100-year return value estimates for ocean wind speed and significant wave height from the ERA-40 data, *J. Clim.*, **18**, 1032–1048.
- Caires, S., A. Sterl, J. R. Bidlot, N. Graham, and V. R. Swail, 2004: Intercomparison of different wind wave reanalysis, *J. Clim.*, **17**, 1893–1913.
- Caires, S., and A. Sterl, 2005: A new non-parametric method to correct model data: Application to significant wave height from the ERA-40 reanalysis, *J. Atmos. Oceanic Tech.*, **22**, 443–459.
- Carter, D. J. T., and L. Draper, 1988: Has the north-east Atlantic become rougher?, *Nature*, **332**, 494.
- Chou, C., J.-Y. Tu, and J.-Y. Yu, 2003: Interannual variability of the western North Pacific summer monsoon: Differences between ENSO and non-ENSO years, *J. Clim.*, **16**, 2275–2287.
- Graham, N. E., and H. F. Diaz, 2001: Evidence for intensification of North Pacific winter cyclones since 1948, *Bull. Amer. Meteor. Soc.*, **82**, 1869–1893.
- Graham, N. E., R. R. Strange, and H. F. Diaz, 2002: Intensification of North Pacific winter cyclones 1948–98: Impacts on California wave climate, Proc. 7th Int. Workshop on Wave Hindcasting and Forecasting, Banff, AB, Canada, U.S. Army Engineer Research and Development Center, 60–69.
- Houghton, J. T., Y. Ding, D. J. Griggs, M. Noguer, P.J. van der Linden, X. Dai, K. Maskell, and C. A. Jhonson, Eds., 2001: Climate change 2001: the scientific basis. Contribution of Working Group I to the Third Assessment Report of the Intergovernmental Panel on Climate Change. Cambridge University Press, 881pp.
- Kako, S., and M. Kubota, 2006: Relationship between an El Niño event and the interannual variability of significant wave heights, *Atmosphere–Ocean*, in press.
- Kalnay et al., 1996: The NCEP/NCAR 40-year reanalysis project, *Bull. Amer. Meteor. Soc.*, **77**, 437–470.
- Kanno, H., 2004: Five-year cycle of north–south pressure difference as an index of summer weather in Northern Japan from 1982 onwards, *J. Met. Soc. Japan*, **82**, 711–724.
- Knutson, T. R., and S. Manabe, 1995: Time-mean response over the tropical Pacific to increased CO₂ in a coupled ocean-atmosphere model, *J. Climate*, **8**, 2181–2199.
- Mitchell, J. F. B., T. C. Johns, J. M. Gregory and S. F. B. Tett, 1995: Climate response to increasing levels of greenhouse gases and sulphate aerosols. *Nature*, **376**, 501–504.
- Nitta, T., 1987: Convective activities in the tropical western Pacific and their impact on the Northern Hemisphere summer circulation. *J. Meteor. Soc. Japan*, **65**, 373–390.
- Queffeuou, P., 1999: Long-term comparison of ERS, TOPEX and POSEIDON altimeter wind and wave measurements, Proc. of the ninth International Offshore and Polar Engineering Conference, ISOPE-99, May 30 – June 4, 1999, Brest, France, Vol. III, 114–120.

- Sasaki, W., S. I. Iwasaki, T. Matsuura, S. Iizuka, and I. Watabe, 2005a: Changes in wave climate off Hiratsuka, Japan, as affected by storm activity over the western North Pacific, *J. Geophys. Res.*, **110**, C09008, doi:10.1029/2004JC002730.
- Sasaki, W., S. I. Iwasaki, T. Matsuura, and S. Iizuka, 2005b: Recent increase in summertime extreme wave heights in the western North Pacific, *Geophys. Res. Lett.*, **32**, L15607, doi:10.1029/2005GL023722.
- Smith, T. M., and R. W. Reynolds, 2004: Improved extended reconstruction of SST (1854-1997), *J. Climate*, **17**, 2466-2477.
- Timmermann, A., J. Oberhuber, A. Bacher, M. Esch, M. Latif and E. Roeckner, 1999: Increased El Niño frequency in a climate model forced by future greenhouse warming, *Nature*, **398**, 694-696.
- Tolman, H. L., 1999: User manual and system documentation of WAVEWATCH-III version 1.18, NOAA/NWS/NCEP Ocean Modeling Branch Contribution 166, 112pp.
- Uppala, S. M., et al., 2005: The ERA-40 reanalysis, *Q.J.R. Meteorol. Soc.*, **131**, 2961-3012, doi:10.1256/QJ.04.176.
- Wang, B. and J. C. L. Chan, 2002: How strong ENSO events affect tropical storm activity over the western North Pacific, *J. Climate*, **15**, 1643-1658.
- Wang, X. L., V. R. Swail, 2001: Changes of extreme wave heights in northern hemisphere oceans and related atmospheric circulation regimes, *J. Climate*, **14**, 2204-2221.
- WASA Group, 1998: Changing waves and storms in the northeast Atlantic? *Bull. Amer. Meteor. Soc.*, **79**, 741-760.
- Woolf, D. K., P. G. Challenor, and P. D. Cotton, 2002: Variability and predictability of the North Atlantic wave climate, *J. Geophys. Res.*, **107**, 3145, doi:10.1029/2001JC001124.
- Yamaguchi, M., and Y. Hatada, 2002: 51-year wave hindcast and analysis of wave height climate trend of the Northwestern Pacific ocean, Proc. 7th Int. Workshop on Wave Hindcasting and Forecasting, Banff, AB, Canada, U.S. Army Engineer Research and Development Center, 60-69.